AIAA JOURNAL
Vol. 48, No. 3, March 2010

Bridging the Gap between Pressure-Sensitive Paint and Balance Measurements

Wim Ruyten*
Euclidean Optics Inc., Tullahoma, Tennessee 37388
and
James H. Bell†
NASA Ames Research Center, Moffett Field, California 94035

DOI: 10.2514/1.38376

We consider the question of how to reconcile integrated forces and moments from a pressure-sensitive paint measurement with measured forces and moments from a balance. We show that it is possible to compute the smallest change in pressure distribution that would be required to bring the two sets of data into agreement. We refer to this as the gap distribution and show that it can be expressed in terms of a set of basis functions that are determined by the geometry of the test article. The use of these gap basis functions allows discrepancies in forces and moments to be expressed in terms of a common unit of measure, namely the magnitude of the implied gap distribution. We apply this gap analysis to data from a wind-tunnel test of the NASA Orion command module, for which both pressure-sensitive paint data and balance data are available. Results of the analysis confirm earlier suspicions that there was a problem with the normal component of force of the balance. Still, it is shown that application of the gap correction leads to improved pressure-sensitive paint data, as determined by the level of agreement with pressure tap data. The analysis procedure involving a pressure-gap distribution should be applicable to the comparison of balance data to integrated forces and moments from computational fluid dynamics calculations and other techniques.

Nomenclature

Alpha, α	=	model pitch angle
$B_{i\mu}$	=	gap basis function for balance component μ and grid point i
CA, CS, CN	=	coefficients for axial force (CA), side force (CS), normal force (CN)
CPM, CYM	=	coefficients for pitching moment (CPM), yawing moment (CYM)
D	=	vehicle diameter (15.157 in.)
$\mathrm{d}P(\mathbf{x})$	=	pressure-gap distribution
fx, fy, fz	=	index of force components along x axis (CA), y axis (CS), and z axis (CN)
mx, my, mz	=	index of moment components about x axis, y axis (coefficient for pitching moment), and z axis (coefficient for yawing moment)
M	=	Mach number
$P(\mathbf{x})$	=	pressure distribution
Q_∞	=	dynamic pressure
Re_D	=	Reynolds number with respect to vehicle diameter
μ	=	index for force or moment component
$\sigma_{\mu\mu}$	=	sensitivity factor associated with gap basis function

1. Introduction

TRADITIONALLY, the development of new air vehicles involves building and testing of a pressure model, also referred to as a loads model, in which hundreds of pressure taps are used to measure the pressure distribution on the proposed vehicle design. The pressure distributions are then integrated to obtain loads on the wings, control surfaces, and so forth, of the proposed vehicle. More recently, pressure-sensitive paint (PSP) techniques have been developed [1,2], which allow pressure distributions to be obtained with much less expensive models earlier in the aircraft design cycle. This use of PSP has reached a maturity level in recent years that appears to indicate that, at least for some applications, the time has arrived that it is no longer necessary to build the expensive pressure models.

Still, some challenges remain, among them validation that forces and moments obtained by integrating the pressure distribution from a PSP measurement match the measured forces and moments from a conventional balance or load cell. The latter technique is quite mature, so the burden of explaining (or defending) any differences falls to the PSP development teams.

Few direct comparisons between integrated PSP data and balance measurements have been published to date. In 1995 Sellers integrated PSP data on the horizontal stabilizer of an F-18 E/F model [3]. The resulting normal force, pitching moment, and hinge moment compared well with the balance data at Mach numbers from 0.85 to 1.2, but less well at Mach 0.6, presumably (as noted by Sellers) due to high noise levels in the PSP data at the higher pressures.

One of the authors of this paper, James Bell, compared integrated PSP and balance data on a semispan commercial transport model in the NASA Ames Research Center Unitary Wind Tunnel and a fighter model in the Arnold Engineering Development Center 16T Wind Tunnel [4]. It was observed that the PSP-integrated normal force results correlated much better with the balance data than did the axial force results. This was attributed (without much evidence) to difficulty in resolving the large pressure gradients at the wing leading edges. Otherwise, this study did relatively little analysis of the sources of deviation between the PSP and balance results [4].

Good agreement between PSP-based and balance-based measurements were also reported by Klein et al. [5] for a Mako fighter jet model, both for the total normal force and for bending moments of a horizontal tail.

There have also been unpublished efforts to make comparisons between integrated PSP data and balance data; we mention two in passing. The first is a large study conducted by researchers at

Presented as Paper 0843 at the 46th AIAA Aerospace Sciences Meeting and Exhibit, Reno, NV, 7–10 January 2008; received 4 May 2008; revision received 20 December 2008; accepted for publication 7 April 2009.

*Engineer Specialist and President. Associate Fellow AIAA.
†Aerospace Engineer, Code AOX, Mail Stop 260-1. Member AIAA.

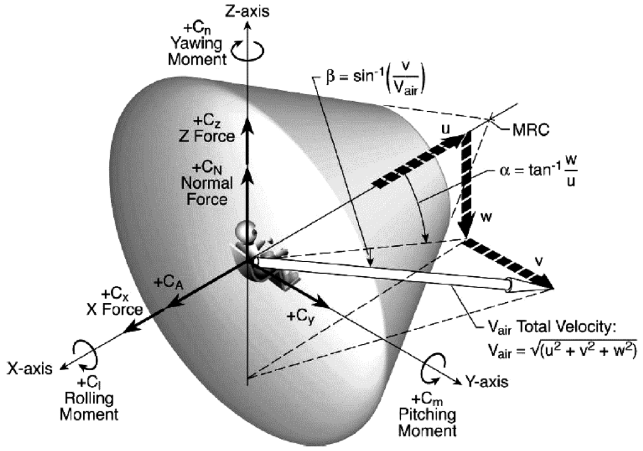

Fig. 1 Coordinate system for Orion Command Module (CEV), with moment reference center at virtual apex (taken from [13] and used with permission.)

McDonnell Douglas on a proprietary model in 1996 [‡]. Bell made an additional unpublished comparison of PSP and balance results on an F-16C model in the NASA Ames Research Center Unitary Wind Tunnel in 2000. This study again showed much better correlation between PSP and balance data for normal force than for axial force.

A large number of studies have been published on the accuracy of PSP in general (see, for example [6–10]), but these have not addressed force and moment integrations specifically. One difficulty has been that few facilities have been equipped to capture the pressure distribution on a sufficiently large part of the surface of the test article to make reliable integrations possible. Tests on complete configurations with balances and/or load cells generally use proprietary models. This accounts for the small number of published studies on this topic. Also, even under optimal circumstances, some interpolation of PSP data is required, particularly around the sting attachment point.

On the other hand, balance data are subject to a number of calibration challenges as well, including, again, the effect of the sting on the measured data and, in the case of a model with internal flow (for example, through inlets), corrections associated with such flow effects.

In this paper, we take a critical look at a set of wind-tunnel data for which both PSP measurements and balance measurements are available. These are data that were acquired on a model of the NASA Orion Command Module [11–14] early in 2006 at the NASA Ames Research Center. (The term Crew Exploration Vehicle [CEV] was still used at the time of the tests.) See Fig. 1 for a sketch of the CEV.

In taking this critical look, we develop (what appears to be) a new technique for comparing balance data with a given pressure distribution. The essence of this technique can be stated as follows. Let $P(\mathbf{x})$ be a pressure distribution on the test article, obtained in some manner, and let an associated set of balance data be given by F_μ, where the index μ can represent any number of measured forces and moments. Then it is possible by strictly mathematical means (that is, without recourse to a physical or aerodynamic model) to compute the smallest change in the distribution $P(\mathbf{x})$, denoted by $\mathrm{d}P(\mathbf{x})$, that would be required to bring the integrated forces and moments into agreement with the balance data F_μ. We refer to this smallest change distribution as the gap distribution. This gap distribution may be interpreted as a bias error distribution, such as discussed, in general terms, by Liu and Finley [15].

There are at least two important applications of such gap analysis. First, in cases where PSP data are believed to have systematic error, inclusion of the gap distribution may be used to improve the PSP data. Second, in cases where problems with the balance data are believed possible, a quantitative answer can be obtained to the question of how much the PSP data would have to be in error to explain the observed discrepancy between integrated PSP data and balance data. In this case, the gap analysis can shed light on which component of the balance data is most likely the cause of the observed discrepancy.

Note that the gap-analysis technique has broad applicability. Though we use it here in conjunction with data from a PSP measurement, the technique might be applied equally well to pressure distributions $P(\mathbf{x})$ obtained using computational fluid dynamics or by other means, for example, by interpolation of pressure tap data.

The organization of this paper is as follows. In Sec. II and Appendix A, we develop the theoretical framework for the computation of the gap distribution. In Sec. III we review a subset of the PSP data and balance data from the CEV test. The gap analysis for this data is performed in Sec. IV. Section V gives a discussion of the results. Section VI states a conclusion.

II. Theoretical Background

A. Calculation of Gap Distribution

Let the pressure distribution on a test article be given by $P(\mathbf{x})$, where $\mathbf{x}$ denotes a point on the surface. Disregarding skin friction (see Sec. III.C), the force $\mathbf{F}$ on the test article and the moment $\mathbf{M}_{\mathrm{ref}}$ about a reference center $\mathbf{x}_{\mathrm{ref}}$ may then be computed as

$$\mathbf{F} = \oint P(\mathbf{x})\,\mathrm{d}\mathbf{A}, \quad \mathbf{M}_{\mathrm{ref}} = \oint P(\mathbf{x})(\mathbf{x} - \mathbf{x}_{\mathrm{ref}}) \otimes \mathrm{d}\mathbf{A} \qquad (1)$$

Here $\mathrm{d}\mathbf{A}$ denotes a surface element, expressed as a vector oriented along the (inward-pointing) surface normal at the point $\mathbf{x}$. The symbol $\otimes$ is used to denote a vector product, with the addition of a minus sign for the resulting rolling moment (about the x axis) and for the yawing moment (about the z axis). The integrals in Eq. (1) are computed over the surface of the test article, which is assumed to be closed.

Assume that the distribution $P(\mathbf{x})$ has been measured using the PSP technique, yielding $P_{\mathrm{PSP}}(\mathbf{x})$, and that substitution of $P_{\mathrm{PSP}}(\mathbf{x})$ into Eq. (1) yields a force $\mathbf{F}_{\mathrm{PSP}}$ and a moment $\mathbf{M}_{\mathrm{PSP}}$. The distribution $P_{\mathrm{PSP}}(\mathbf{x})$ may include interpolated values in areas that were not accessible to any of the PSP cameras, areas with missing paint, and virtual areas such as the sting attachment region.

Assume also that balance data are available, giving a force $\mathbf{F}_{\mathrm{bal}}$ (with indices fx, fy, and fz) and a moment $\mathbf{M}_{\mathrm{bal}}$ (with indices mx, my, mz). We may then express the difference between the two sets of data as

$$\mathrm{d}F_\mu \equiv F_{\mathrm{bal},\mu} - F_{\mathrm{PSP},\mu}, \qquad \mu = fx, fy, fz, mx, my, mz \qquad (2)$$

We use the symbol F_μ for both forces and moments, with the index μ identifying a specific component of force or moment, as indicated.

To find the smallest change in pressure distribution $\mathrm{d}P(\mathbf{x})$ that would account for the observed difference $\mathrm{d}F_\mu$, we use the method of Lagrange multipliers. This allows for the minimization of a cost function (here, the rms magnitude of the pressure-gap distribution) while satisfying the constraint that the integrated forces and moments must match the balance data. In Appendix A, it is shown that the resulting gap distribution can be expressed as follows.

Let i denote an index on the 3-D grid on which the PSP pressure distribution has been measured. Then the discretized form of the gap distribution $\mathrm{d}P(\mathbf{x})$ can be calculated from the measured discrepancies $\mathrm{d}F_\mu$ according to

$$\mathrm{d}P_i = \sum_\mu B_{i\mu} dF_\mu \qquad (3)$$

The terms $B_{i\mu}$ are gap basis functions that are determined by the geometry of the test article, the selection of the moment reference center (MRC) and (to a small extent) the discretization scheme for the force and moment integrations. In essence, the basis functions $B_{i\mu}$ define the inverse of Eq. (1), to the (very limited) extent that a detailed pressure distribution can be reconstructed from a small set of balance components. The calculation of the basis functions $B_{i\mu}$ is discussed in Appendix A.

[‡]Private communication with R. Crites, 1996.

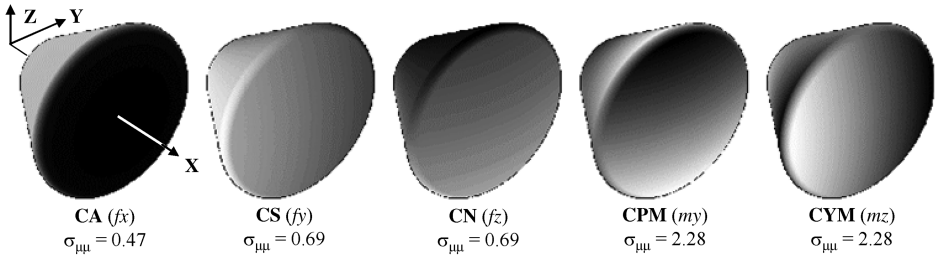

Fig. 2 Gap basis functions for the CEV test article, computed using the GRC as the MRC, with associated sensitivity factors $\sigma_{\mu\mu}$. There is no basis function for rolling moment. Light and dark areas correspond to high and low pressure, respectively.

Figure 1 shows the coordinate system for the CEV test article, with the MRC at the virtual apex of the cone section. Figure 2 illustrates the associated gap basis functions, computed using for the MRC the gap reference center (GRC) of the test article, which is located near the center of gravity and is defined in Sec. II.B. Shown in Fig. 2 from left to right are the basis functions for axial force (along the x axis), side force (along the y axis), normal force (along the z axis), pitching moment (about the y axis), and yawing moment (about the z axis). Because the CEV test article is an axisymmetric body, it is not in fact possible to compute a meaningful basis function for rolling moment about the x axis, as is explained at the end of Appendix A. This is not an issue in the CEV case, because both the PSP technique and the balance data produced values of the rolling moment that are essentially zero. Also, because of the symmetry of the test article, the basis functions for the side component of force (CS) and normal component of force (CN) are equal within a 90-deg rotation about the x axis, as are the basis functions for the coefficients for pitching moment (CPM) and yawing moment (CYM).

In Fig. 2, it is easy to see that a pressure distribution corresponding to one of the basis functions (with light and dark regions representing high and low pressure, respectively) produces precisely the force or moment contribution corresponding to that basis function. In this regard, it may be useful to think of the gap basis functions as a weighting scheme. Pressure applied to a surface element oriented perpendicular to the x axis will have a greater effect on F_x than the same pressure applied to a nonperpendicular surface element. A scheme that minimizes the overall pressure change to achieve a given $\mathrm{d}F_x$ will thus apply pressure preferentially to surface elements perpendicular to the x axis.

Having computed the gap distribution $\mathrm{d}P(\mathbf{x})$ in the form of Eq. (3), a corrected PSP pressure distribution $P'_{\mathrm{PSP}}(\mathbf{x})$ can be computed from the original distribution $P_{\mathrm{PSP}}(\mathbf{x})$ according to

$$P'_{\mathrm{PSP}}(\mathbf{x}) = P_{\mathrm{PSP}}(\mathbf{x}) + \mathrm{d}P(\mathbf{x}) \tag{4}$$

By the very construction of this corrected distribution, it will yield, upon integration, forces and moments that match the balance data exactly.

B. Magnitude of Pressure-Gap Distribution

For analysis purposes, it will prove useful to assess the rms magnitude of the computed gap distribution $\mathrm{d}P(\mathbf{x})$. This magnitude $\sigma_{\mathrm{d}P}$ may be computed from the terms $\mathrm{d}P_i$ in Eq. (3) according to

$$\sigma_{\mathrm{d}P} \equiv \left[\sum_i \mathrm{d}P_i^2 \mathrm{d}S_i / \sum_i \mathrm{d}S_i\right]^{1/2} \tag{5}$$

Here, the weighting factor $\mathrm{d}S_i$ denotes the magnitude of the surface area (for example, with units of square inches) of a surface element $\mathrm{d}\mathbf{A}_i$ in Eq. (1).

The result from Eq. (5) may be applied directly in practice. Still, it is instructive to show the relationship of the rms magnitude of the gap distribution to the measured discrepancies in forces and moments $\mathrm{d}F_\propto$ from Eq. (2). This relationship is found by substituting Eq. (3) into Eq. (5), yielding

$$\sigma_{\mathrm{d}P}^2 = \sum_\mu \sum_\nu \sigma_{\mu\nu}^2 \mathrm{d}F_\mu \mathrm{d}F_\nu \tag{6}$$

The terms $\sigma_{\sigma\nu}^2$ in Eq. (4) constitute a covariance matrix, with elements

$$\sigma_{\mu\nu}^2 = \sum_i B_{i\mu} B_{i\nu} dS_i / \sum_i \mathrm{d}S_i \tag{7}$$

Like the basis functions $B_{i\mu}$ themselves, this covariance matrix depends strictly on the geometry of the test article and is independent of the measured data. Rather, the covariance matrix determines how discrepancies in the measured data are translated into an rms magnitude of the implied pressure-gap distribution.

If the basis functions $B_{i\mu}$ are orthogonal (in the sense that $\sum_i B_{i\mu} B_{i\nu} \mathrm{d}S_i = 0$ when $\propto \neq \nu$), the result from Eq. (6) can be simplified to

$$\sigma_{\mathrm{d}P}^2 = \sum_\mu \sigma_{\mu\mu}^2 \mathrm{d}F_\mu^2 \tag{8}$$

For the CEV test article, this orthogonality was achieved by moving the MRC along the x axis until the off-diagonal elements of the covariance matrix vanished. This occurred at an axial location given by $\mathbf{x}_{\mathrm{GRC}} = (x_{\mathrm{GRC}}, 0, 0)$, with $x_{\mathrm{GRC}}/D = 0.7304$. We refer to this choice of MRC as the GRC.

Assuming an orthogonal choice of basis functions, we may assess the relative contribution of each balance component to the computed pressure-gap distribution. To do this, we define [cf. Eq. (8)] partial rms pressure-gap magnitudes according to

$$\sigma_{\mathrm{d}P,\mu} = \sigma_{\mu\mu} |\mathrm{d}F_\mu|, \qquad \text{each } \mu \tag{9}$$

This result shows that the geometric quantities $\sigma_{\mu\mu}$ may be thought of as (dimensionless) sensitivity factors, by which discrepancies in force or moment measurements are converted to an rms magnitude of the corresponding pressure-gap distribution.

Figure 2 shows the sensitivity factors $\sigma_{\mu\mu}$ for each of the five basis functions for the CEV test article, assuming that pressures, forces, and moments are expressed as dimensionless coefficients (see Sec. III). The axial force has a smaller sensitivity factor than the side and normal forces, and the moments have sensitivities more than three times those for CS and CN.

III. Review of Crew Exploration Vehicle Data

The data set under consideration is that from a test of a 7.7% scale model of the NASA Orion Command Module, which was tested in the NASA Ames Research Center Unitary Project 11-ft Transonic Wind Tunnel in February and March 2006. Data from the test were documented before [11–13] and are reviewed here only to the extent necessary for conducting a comparison of PSP data and balance data for a subset of the data.

A. Balance Data

The test article was equipped with the NASA Ames Research Center task balance MK13A mounted internal to the model, at an angle of 135 deg relative to the chassis. This is a six-component balance that was calibrated using procedures described in NASA document A307-9865-XM1, Rev. 1. Drift corrections of up to 0.25% of full scale were performed by interpolating data between zeroes that were acquired at regular intervals. Cavity pressures were measured,

and a small correction was performed for cavity pressure effects. Additional information may be found in [11,13].

Both force and moment data were scaled to dimensionless coefficients, according to

$$C_{F,\mu} = F_\mu/(Q_\infty A_{\text{ref}}), \qquad C_{M,\mu} = M_\mu/(Q_\infty A_{\text{ref}} L_{\text{ref}}) \tag{10}$$

Here, A_{ref} is the reference area of the test article, given in terms of the vehicle diameter D by $A_{\text{ref}} = (\pi/4)D^2$ and L_{ref} is a reference length, given by $L_{\text{ref}} = D$. Moment data were originally computed using the virtual apex of the test article as the MRC (see Fig. 1), but were transformed to the GRC as defined in Sec. II.A. Measured force and moment coefficients for selected runs are shown as solid symbols in Figs. 3 and 4 (displayed CN values in Fig. 3 are offset by −0.4 for clarity). Rolling moments were measured but were negligible, as is expected for a circularly symmetric test article.

Based on prior analysis [11], there was some indication that the measured normal force of the balance was too high (by up to 0.015 units of CN), particularly at small Mach numbers ($M = 0.5$).

B. Pressure-Sensitive Paint Data

Pressure-sensitive paint data were acquired using the portable, lifetime-based PSP system that was developed at the Arnold Engineering Development Center under the direction of Marvin Sellers of Aerospace Testing Alliance [14]. Four CoolSNAP K4 cameras were used to obtain near-complete coverage of the test article. (Data at the highest two model alphas had a small unmapped area and are not included in the present analysis.) Illumination was achieved with 16 banks of 465-nm light-emitting diodes, pulsed at 600-μ sec intervals. Images were acquired at two gates with respect to the train of excitation pulses. Data were processed by performing black subtraction, bias correction, ratioing, patching over targets, mapping to a 3-D grid, and converting signal ratios to pressures. In this last step, data from up to 153 pressure taps were used to achieve an in situ calibration of the paint for each run point.

Most aspects of the PSP data reduction process have been presented before [16,17]. The bias correction scheme is an exception because it has not, thus far, been approved for public release. In essence, this scheme consists of removing pressure-independent contributions due to nonuniform paint response, spectral leakage, and other artifacts. Some of these artifacts have recently been discussed by Goss et al. [18].

Processed PSP data were expressed as pressure coefficients, defined in terms of the local surface pressure P, the freestream pressure P_∞, and the dynamic pressure Q_∞, according to

$$c_p = (P - P_\infty)/Q_\infty \tag{11}$$

Figure 5 shows representative PSP data at Mach numbers of 0.95 and 0.50. Note that, for each Mach number, the pressure distribution is only mildly sensitive to Reynolds number. Just visible in the top of Fig. 5 is a circular area with unmapped data around the sting attachment point. When performing force and moment integrations, pressure in this area was set equal to the value at a nearby pressure tap.

Results of the force and moment integrations are shown as open symbols in Figs. 3 and 4. Good agreement with the balance data is found at $M = 0.95$ (Figs. 3a and 4a), where pressure is low and PSP signal-to-noise ratio is high. More significant deviations are found at $M = 0.5$ (Figs. 3b, 3c, 4b, and 4c), where the pressure is higher and the PSP signal-to-noise ratio lower. At the same time, the observed discrepancy in normal force between the integrated PSP data and the balance data is consistent (in both sign and magnitude) with the suspected error in the balance data for this component.

Aspects of the pressure integration scheme itself are described in [5].

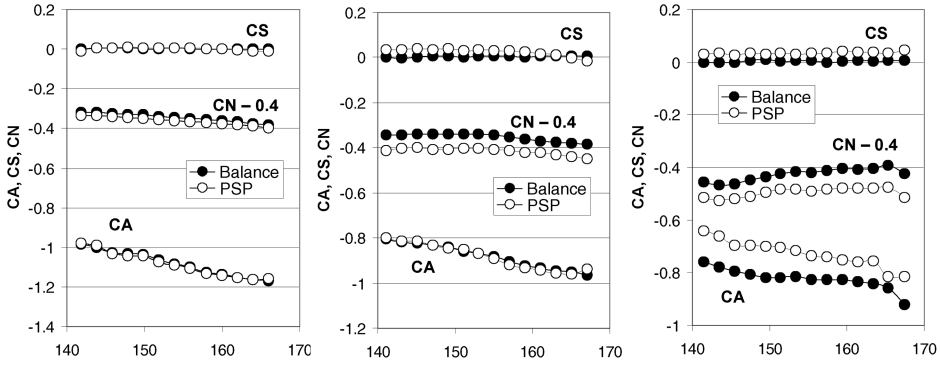

Fig. 3 Measured force coefficients (balance and PSP) for selected runs: a) $M = 0.95$, $Q = 496$ psf, $Re_D = 3.8 \times 10^6$; b) $M = 0.5$, $Q = 117$ psf, $Re_D = 1.5 \times 106$; c) $M = 0.5$, $Q = 308$ psf, $Re_D = 3.8 \times 106$.

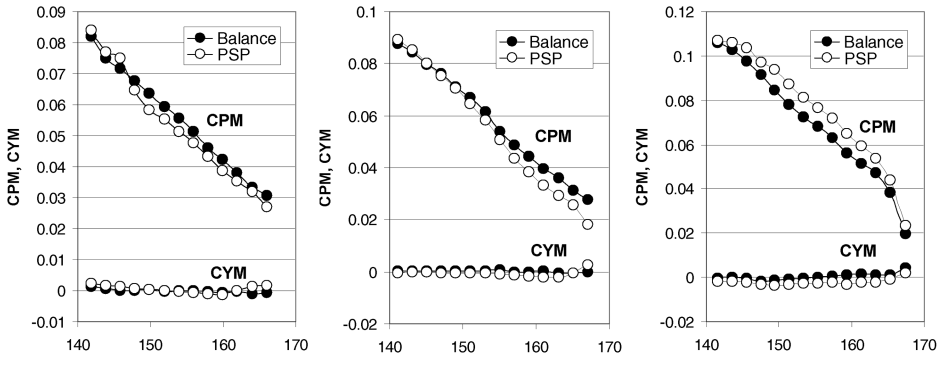

Fig. 4 Measured moment coefficients (balance and PSP) for same runs as in Fig. 3.

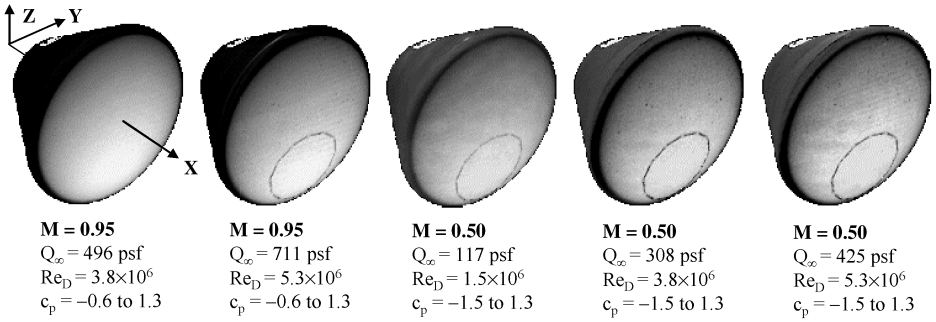

Fig. 5 Representative PSP results for a model alpha of 155 deg, with associated test conditions and c_p ranges shown. Light and dark areas correspond to high and low pressure, respectively.

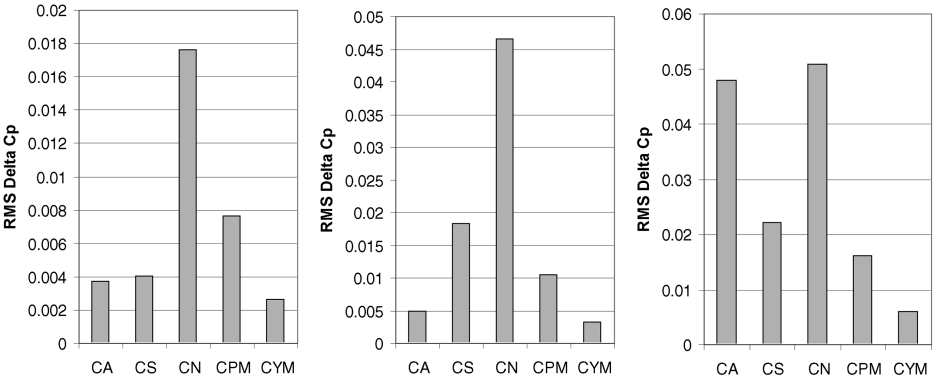

Fig. 6 Component-specific rms magnitudes of computed pressure-gap distributions (averaged over model alpha) for same runs as in Figs. 3 and 4.

C. Effect of Skin Friction

Even under the best of circumstances, integrated PSP data are not expected to match data from a balance exactly because the PSP data are (believed to be) insensitive to shear forces at the surface of the test article. In the case of the CEV data, the effect of shear is believed to be small based on the predictions from computation fluid dynamics codes. When Navier–Stokes simulations were used to calculate the forces and moments for the CEV, the results differed by less than 1% depending on whether or not surface shear values were included in the integrations[§].

In other cases, it may be possible to estimate the skin friction drag using numerical simulation. Also, techniques are being developed to measure skin friction experimentally [19].

IV. Results of Gap Analysis

To apply the pressure-gap corrections from Sec. II and Appendix A to the CEV PSP data, modifications were made to the software module that was used to perform the force and moment integrations of the PSP data. First, the gap basis functions were computed. These have already been shown in Fig. 2. Next, discrepancies between integrated PSP data and balance data from Eq. (2) were converted to a gap distribution using Eq. (3). Root mean square magnitudes of the resulting gap distributions were computed using Eq. (5). Partial rms contributions to the gap distributions for individual balance components were computed using Eq. (9). We present the latter results first, in the form of Fig. 6.

Shown in Fig. 6 are the rms magnitudes of the computed pressure-gap corrections (in units of c_p) for individual balance components, using the data from Figs. 3 and 4. Within each run, results were averaged over the attitude angle α. As expected, the largest contribution to the gap distributions are computed for those balance components for which the integrated PSP data differ substantially from the balance data. Thus, large values of $\sigma_{dp,\mu}$ are found for CN in Figs. 6a–6c and for CA in Fig. 6c. The rms gap error $\sigma_{dp,\mu}$ for CPM is significantly smaller than for the normal force. Based on a visual inspection of Figs. 3 and 4 this result may be surprising, but is a direct consequence of the fact that moment values and force values transform to a pressure-gap distribution differently.

Composite rms measures of the computed gap distribution (i.e., including corrections for each of the balance components) are shown in Fig. 7. These rms gap magnitudes were computed using Eq. (5) and are denoted as RmsGap in Fig. 7 [it was verified that equal results can be obtained using Eq. (8).] To help interpret the magnitudes of the resulting gap distributions, two other quantities are shown in Fig. 7. These are the rms differences between the PSP data in the vicinity of roughly 140 pressure taps (after culling) and the readings from these taps, both before (RmsTap1) and after (RmsTap2) application of the pressure-gap correction. Omitted (culled) from the calculation of RmsTap1 and RmsTap2 were taps with deviations outside plus or minus three standard deviations (typically from 6 to 12 taps out of the 153 taps available).

In Fig. 7, it is seen that application of the gap correction generally improves the agreement with the pressure taps (i.e., RmsTap2< RmsTap1), but generally does not produce RmsTap2 values smaller than the rms magnitude of the computed gap distribution itself. This behavior was also found for other runs that are not included in the results from Fig. 7. Corrected pressure distributions for the data from Fig. 5 are not shown explicitly because they differ from the data in Fig. 5 only in a small way.

V. Discussion

From the analysis in Sec. IV it appears that both the PSP data and the balance data have errors associated with them. Errors in the PSP data are evident from the fact that the PSP data deviate from the pressure tap values in the amount of the quantity RmsTap1 in Fig. 7. Errors in the balance data are particularly noticeable in the normal component of force. Indeed, integrated PSP results confirm earlier suspicions (see [11,13,20]) that the measured CN component of the balance tends to be too large, particularly at low Mach numbers. This is the most likely explanation for the fact that in Fig. 6, the CN component consistently yields the largest pressure-gap correction. It also explains why the RmsTap2 values in Fig. 7 (i.e., the

[§]Private communication with M. E. Olson and S. Rogers, May 2007.

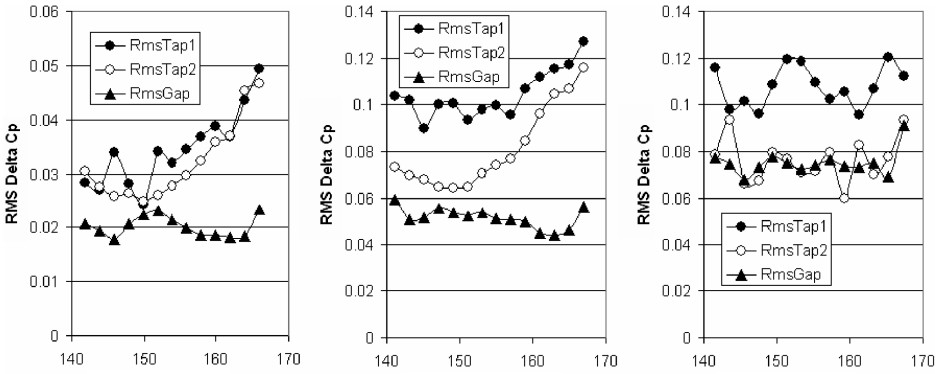

Fig. 7 Comparison of rms magnitudes of pressure-gap distributions with rms deviations between PSP and pressure taps, both before (RmsTap1) and after (RmsTap2) gap correction, for same runs as in Figs. 3–5.

disagreement between PSP data and pressure taps following the gap correction) generally do not fall below the rms magnitude of the computed gap correction itself.

To understand why this would be the case, consider a hypothetical case in which the PSP data match the tap data exactly, but the balance data are in error. In this case, the rms magnitude of the computed pressure-gap correction will be precisely equal to the rms difference between the corrected PSP data and the pressure taps (assuming the presence of many taps across the surface).

Despite the complication posed by the likely errors in the balance data it appears that, especially at low Mach number (where the PSP data suffer from low signal-to-noise ratio), the pressure-gap correction does improve the PSP data overall, as evidenced by the improved agreement with the pressure taps.

VI. Conclusions

We have shown that there is a novel technique for comparing data from a PSP measurement to force and moment measurements that are obtained by a balance. The technique involves the computation of a set of gap basis functions that are determined by the geometry of the test article. These basis functions can be used, in turn, to compute the smallest change in pressure distribution (the gap distribution) that would be required to reconcile the differences between the PSP data and the balance data.

Although the computed gap distribution may not be physical (or aerodynamic) in nature, it allows an assessment to be made of the relative accuracies of the PSP data versus the balance data. In particular, it allows discrepancies in force and moment data to be evaluated using a common unit of measure, namely the rms magnitude of the implied pressure-gap distribution. As such, it may also serve as one more method to quantify the error in PSP data [21].

The gap-analysis technique was applied to data from a wind-tunnel test of the NASA Orion Command Module (the CEV), for which both PSP data and balance data were available. Data from selected runs were analyzed using the newly developed gap-analysis scheme. The results suggest that there were consistent problems with the normal force component of the balance, as was already suspected based on prior analysis. Nevertheless, it is shown that application of the pressure-gap correction generally leads to an improved level of agreement between the PSP results and pressure taps in the model.

The gap-analysis method that has been developed should be applicable to other techniques in which full-field pressure distributions are determined and need to be compared with balance data. This would be true, in particular, for pressure distributions computed using computational fluid dynamic results.

Appendix A: Computation of Gap Basis Functions

To see how Eq. (3) comes about, we discretize Eq. (1) as follows:

$$F_\mu = \sum_i P_i \mathrm{d}A_{i\mu}, \qquad \mu = fx, fy, fz, mx, my, mz \tag{A1}$$

Here, the sum over i replaces the integrals in Eq. (1) and the index μ includes forces and moments as indicated, using redefinitions of the elements $dA_{i\mu}$ as appropriate for moment components.

The difference in balanced-based and PSP-based measurements $\mathrm{d}F_\mu$ from Eq. (2) may now be expressed as

$$\phi_\mu \equiv \sum_i \mathrm{d}P_i \mathrm{d}A_{i\mu} - \mathrm{d}F_\mu = 0, \qquad \text{each} \tag{A2}$$

To find the gap distribution $\mathrm{d}P_i$ that is minimal in a least-squares sense, we wish to minimize the rms magnitude of the pressure-gap distribution, which [see Eq. (5)] is proportional to the quantity

$$\phi_{\text{gap}} \equiv \sum_i \mathrm{d}P_i^2 \mathrm{d}S_i \tag{A3}$$

Here, $\mathrm{d}S_i$ denotes the area magnitude of the i-th surface element $\mathrm{d}\mathbf{A}$ in Eq. (1). Inclusion of the terms $\mathrm{d}S_i$ in Eq. (A3) ensures that the calculation of the gap distributions $\mathrm{d}P_i$ is insensitive to variations in grid spacing across the surface of the test article.

The minimization of Eq. (A3) is not performed freely, but is constrained by Eq. (A2). Such a minimization calls for the method of Lagrange multipliers in which a new cost function is introduced, in this case

$$\phi \equiv \phi_{\text{gap}} + 2\sum_\mu \lambda_\mu \phi_\mu \tag{A4}$$

Here, the functions ϕ_{gap} and ϕ_μ are those from Eqs. (A2) and (A3), and the coefficients λ_μ are Lagrange multipliers that are to be determined along with the distribution $\mathrm{d}P_i$. The factor 2 in Eq. (A4) is for notational convenience in the remainder of Appendix A.

Setting the partial derivatives of Eq. (A4) to zero with respect to $\mathrm{d}P_i$ leads to

$$\mathrm{d}P_i \mathrm{d}S_i + \sum_\mu \lambda_\mu \mathrm{d}A_{i\mu} = 0, \qquad \text{each } i \tag{A5}$$

This set of equations must be solved along with the set of equations that is expressed by Eq. (A2).

The terms $\mathrm{d}P_i$ can be eliminated initially from Eqs. (A2) and (A5) to arrive at the following system of equations for the Lagrange multipliers λ_μ alone

$$\sum_\nu C_{\mu\nu}\lambda_\nu = -\mathrm{d}F_\mu, \quad C_{\mu\nu} \equiv \sum_i \frac{\mathrm{d}A_{i\mu}\mathrm{d}A_{i\nu}}{\mathrm{d}S_i} \tag{A6}$$

Formally, we may write the solution of this system as

$$\lambda_\mu = -\sum_\nu C^{-1}_{\mu\nu} \mathrm{d}F_\nu \tag{A7}$$

Here $C^{-1}_{\mu\nu}$ is element (μ, ν) of the inverse of the matrix $\mathbf{C}$ that is implied by the elements $C_{\mu\nu}$ in Eq. (A6). Substituting the result from

Eq. (A7) back into Eq. (A5) allows us to solve for the gap distribution $\mathrm{d}P_i$ according to

$$\mathrm{d}P_i = \sum_{\mu}\sum_{\nu}\frac{\mathrm{d}A_{i\mu}}{\mathrm{d}S_i}C^{-1}_{\mu\nu}\mathrm{d}F_{\nu} \equiv \sum_{\nu}B_{i\nu}\mathrm{d}F_{\nu} \tag{A8}$$

The far right-hand side of Eq. (A8) is precisely the result from Eq. (3) in Sec. II, upon reversing indices μ and ν.

From Eq. (A8) it follows that the terms $B_{i\propto}$ from Eq. (3) in Sec. II are given by

$$B_{i\mu} = \sum_{\nu}\frac{\mathrm{d}A_{i\nu}}{\mathrm{d}S_i}C^{-1}_{\nu\mu} \tag{A9}$$

Formally, the implied matrix $\mathbf{B}$ may be expressed as $\mathbf{B} = \mathbf{A}\mathbf{C}^{-1}$, where $\mathbf{C}$ denotes the matrix implied by the elements $C_{\mu\nu}$ from Eq. (A6). In practice, it is convenient to compute $\mathbf{B}$ by solving the matrix equation $\mathbf{C}\mathbf{B} = \mathbf{A}$, for example, using Cholesky decomposition of the matrix $\mathbf{C}$. The relationship of the matrix $\mathbf{B}$ (or, more precisely, its transpose) to the matrix $\mathbf{A}$ is essentially that of a so-called Moore–Penrose pseudoinverse [22].

The matrix $\mathbf{B}$ is determined strictly by the geometry of the test article, the selection of the MRC for the moment computations, and (to a small degree) the discretization scheme used for the force and moment calculations. The dependence on the discretization scheme is minimized by the inclusion of the terms $\mathrm{d}S_i$ in Eq. (A3).

In general, one basis function can be computed for each moment component of the balance. When this was done for the CEV test article, it was found that the basis function for rolling moment about the x axis was essentially zero for more than 99% of the surface, and equal to a large value along the edges of some of the grid boundaries. This may be understood as the impossibility of defining a meaningful roll basis function for a circularly symmetric test article. Although it might be possible to define a pressure distribution that produces a rolling moment, there is, based on geometry alone, no preferred azimuthal orientation for such a distribution due to the circular symmetry of the surface. This means that for the CEV case, the numerically computed gap basis function for the rolling moment is determined strictly by rounding errors. For this reason, it was dropped from the analysis in Secs. II, III, and IV.

Appendix B: Corrections Relative to AIAA Paper 2008-843

In preparing the current manuscript, several corrections were made relative to the original conference paper. The first is the calculation of the gap basis functions: In Appendix A, Eq. (A3) now uses scaling by terms $\mathrm{d}S_i$ (vs $\mathrm{d}S_i^2$). This results in slightly modified basis functions, a slightly modified GRC, and thus slightly modified values of the transformed moments. Most importantly, not only are the basis functions themselves insensitive to variations in grid spacing across the surface, but so are the calculated pressure-gap distributions. This is because Eq. (3) in Sec. II.A no longer includes scaling by the area elements $\mathrm{d}S_i$.

The second correction pertains to Eq. (2), which had a sign error resulting in a sign error in the calculation of the pressure-gap correction in Eq. (3). Consequently, for most data it is now found that application of the gap correction improves the agreement between the PSP data and the pressure taps.

Finally, in reporting rms differences between PSP data and tap data, data points outside a three-sigma threshold were culled (typically from 6 to 12 taps out of the 153 taps on the CEV model). This resulted in lower rms tap values, both before and after application of the gap correction.

Acknowledgments

The authors would like to thank Marvin Sellers of Aerospace Testing Alliance for discussions and assistance. We also thank Mike Olson and Stuart Rogers of NASA Ames Research Center for estimates of the possible effects of skin friction on the Crew Exploration Vehicle data.

References

[1] Bell, J. H., Schairer, E. T., Hand, L., and Mehta, R. D., "Surface Pressure Measurements Using Luminescent Coatings," *Annual Review of Fluid Mechanics*, Vol. 33, No. 1, 2001, pp. 155–206. doi:10.1146/annurev.fluid.33.1.155

[2] Liu, T., and Sullivan, J., *Pressure and Temperature Sensitive Paints*, Springer, Berlin, 2005.

[3] Sellers, M. E., "Demonstrations of a Pressure Sensitive Paint Data System in the AEDC Propulsion Wind Tunnel 16T," Arnold Engineering Development Center, Rept. AEDC-TR-95-8, Arnold Air Force Base, TN, Oct. 1995.

[4] Bell, J. H., "Force and Moment Measurements with Pressure-Sensitive Paint," *1999 World Aviation Congress*, Society of Automotive Engineers, Paper 1999-01-5601, Warrendale, PA, Oct. 1999.

[5] Klein, C., Engler, R. H., Henne, U., and Sachs, W. E., "Application of Pressure-Sensitive Paint for Determination of the Pressure Field and Calculation of the Forces and Moments of Models in a Wind Tunnel," *Experiments in Fluids*, Vol. 39, No. 2, Aug. 2005, pp. 475–483. doi:10.1007/s00348-005-1010-8

[6] Goss, L. P., Trump, D. D., Sarka, B., Lydick, L. N., and Baker, W. M., "Multi-Dimensional Time-Resolved Pressure-Sensitive-Paint Techniques: A Numerical and Experimental Comparison," AIAA Paper 2000-0832, Jan. 2000.

[7] Liu, T., Guille, M., and Sullivan, J. P., "Accuracy of Pressure-Sensitive Paint," *AIAA Journal*, Vol. 39, No. 1, 2001, pp. 103–112. doi:10.2514/2.1276

[8] Kammeyer, M., Donovan, J., Kelbe, C., Benne, M., Kihlken, T., and Felter, J. A., "Accuracy Assessment of a Pressure-Sensitive Paint Measurement System," AIAA Paper 2002-0530, Jan. 2002.

[9] Puklin, E., Carlson, B., Gouin, S., Costin, C., Green, E., Ponomarev, S., Tanji, H., and Gouterman, M., "Ideality of Pressure-Sensitive Paint. I. Platinum Tetra (Pentafluorophenyl) Porphine in Fluoroacrylic Polymer," *Journal of Applied Polymer Science*, Vol. 77, No. 13, 2000, pp. 2795–2804. doi:10.1002/1097-4628

[10] Kurita, M., Nakakita, K., Mitsuo, K., and Watanabe, S., "Temperature Correction of Pressure-Sensitive Paint for Industrial Wind Tunnel Testing," *AIAA Journal*, Vol. 43, No. 5, 2006, pp. 1499–1505.

[11] Bell, J. H., "Transonic/Supersonic Wind Tunnel Testing of the NASA Orion Command Module," AIAA Paper 2007-1006, Jan. 2007.

[12] Bell, J. H., and Murphy, K. J., "Comparison of Crew Exploration Vehicle (CEV) Tests in Two Supersonic Wind Tunnels," AIAA Paper 2007-1008, Jan. 2007.

[13] Bell, J. H., "Test 5-CA Final Rept.," Crew Exploration Vehicle Program (Project Orion) Rept. EG-CEV-06-19, March 2006.

[14] Sellers, M., "AEDC's Portable Pressure-Sensitive Paint Data Acquisition System," AIAA Paper 2007-1606, Feb. 2007.

[15] Liu, T., and Finley, T., "Estimating Bias Error Distributions," *Review of Scientific Instruments*, Vol. 72, No. 9, Sept. 2001, pp. 3561–3571. doi:10.1063/1.1394188

[16] Ruyten, W., and Sellers, M., "On-Line Processing of Pressure-Sensitive Paint Images," *Journal of Aerospace Computing, Information, and Communication*, Vol. 1, No. 9, Sept. 2004, pp. 372–382. doi:10.2514/1.8587

[17] Ruyten, W., and Sellers, M., "Improved Data Processing for Pressure-Sensitive Paint Measurements in an Industrial Facility," AIAA Paper 2006-1042, Jan. 2006.

[18] Goss, L. P., Crafton, J. W., Jones, E. G., and Forlines, R. A., "Lifetime Based Pressure Sensitive Paint Systems: Issues and Solutions," *22nd International Congress on Instrumentation in Aerospace Simulation Facilities*, IEEE Publications, Piscataway, NJ, June 2007.

[19] Liu, T., Montefort, J., Woodiga, S., Merati, P., and Shen, L., "Global Luminescent Oil-Film Skin-Friction Meter," *AIAA Journal*, Vol. 46, No. 2, Feb, 2008, pp. 476–485. doi:10.2514/1.32219

[20] Ruyten, W. M., and Bell, J. H., "Bridging the Gap Between Pressure-Sensitive Paint and Balance Measurements," AIAA Paper 2008-0843, Jan. 2008.

[21] Ruyten, W. M., "Full-Field Uncertainty Determination for Pressure-Sensitive Paint Measurements," *AIAA Journal*, Vol. 46, No. 5, May 2008, pp. 1266–1268. doi:10.2514/1.32127

[22] Ben-Israel, A., and Greville, T. N. E., *Generalized Inverses: Theory and Applications*, Wiley, New York, 1977.

K. Asai
Associate Editor